



Supplementary Materials for

Rapid Soil Production and Weathering in the Western Alps, New Zealand

Isaac J. Larsen,* Peter C. Almond, Andre Eger, John O. Stone,
David R. Montgomery, Brendon Malcolm

*To whom correspondence should be addressed. E-mail: larseni@caltech.edu

Published 16 January 2014 on *Science Express*
DOI: 10.1126/science.1244908

This PDF file includes:

Materials and Methods
Supplementary Text
Figs. S1 to S7
Tables S1 to S7
References

Materials and Methods

Soil, bedrock, and sediment sampling

We sampled soil from five ridges in the western Southern Alps (Fig. S2, S3). To avoid sampling material that experienced geochemical alteration during downslope transit (33, 34), soils were collected from the main ridge or from local, meter-scale convexities on smaller divides emanating from the main ridge, rather than downslope locations. The morphology and horizon development of each soil was described prior to sampling. We discarded organic-rich O-horizon materials and collected material generally from the entire soil column; from the top of the A-horizon down to the parent material. The depth to bedrock (mineral soil thickness) was measured at each site. Soil bulk density was estimated using the compliant cavity method (35). Local slope at each site was measured with a clinometer. Bedrock was sampled from the lowermost depth of each soil pit, which reached into fractured rock, as well as from the nearest outcrop to each pit. At one soil pit (Alex Knob Pit 4) we collected soil in 10 cm thick increments, which correspond closely to the soil horizons at the site (Fig. S4). We collected one sample from a bedrock outcrop in the Karangarua catchment. We also collected sand-sized river sediment from sandbars and channel margin deposits.

Sample processing and analysis

All samples were wet sieved to isolate the 250–850 μm grain-size fraction. The 250-850 μm grain-size fraction was treated with warm HCl for 24 h, followed by treatment with a combination of warm NaOH and H₂O₂ for 24 h; both treatments were then repeated. Selective dissolution in 2% HF was used to isolate quartz. Refractory heavy minerals were removed using lithium heteropolytungstate (LST) heavy liquid. A surfactant was used to aid removal of muscovite and feldspar. Samples were boiled in NaOH prior to the final HF etch. ⁹Be carrier was added to quartz aliquots prior to dissolution and Be separation at the University of Washington Cosmogenic Isotope Laboratory (36, 37). BeO was packed into cathodes with Nb powder and ¹⁰Be/⁹Be ratios were measured via accelerator mass spectrometry (AMS) at Lawrence Livermore National Laboratory.

Splits of each bulk soil sample (generally ~1 kg) were crushed and pulverized. Zirconium (Zr) concentrations were measured on sub-splits of the pulverized material. Loss-on-ignition (LOI) was also measured for sub-splits and soil Zr concentrations were corrected for LOI. Surfaces of bedrock samples were cut or ground off to remove potentially weathered joint or foliation surfaces prior to Zr measurement. Bedrock density was measured following the removal of joint surfaces by weighing samples in air and in water. All Zr measurements were made via x-ray fluorescence on pressed powder samples at ALS Minerals, Vancouver, Canada. We generally calculated the chemical depletion fraction (CDF) (18, 38) using the bedrock collected from the base of each pit, rather than bedrock collected from outcrops, because preliminary measurements of the outcrop samples suggested Zr concentrations were spatially variable, which has been observed in other studies (39). However, the Gunn Pit 4 and Gunn Pit 6 rock samples from the base of the soil pits had higher Zr concentrations than the soil, so we used Zr

concentrations in bedrock from outcrops to calculate the CDF for those sites. Bedrock weathering beneath the soil would lead to the interpretation that the CDF are minimum values, but bedrock density values suggest relatively little mass loss due to incipient saprolite formation (Table S1). Soil oxide percentages were measured via x-ray fluorescence on fused samples by ALS Minerals, Vancouver, Canada. We used oxide data to calculate the Chemical Index of Alteration (CIA), as $CIA = [Al_2O_3 / (Al_2O_3 + CaO + K_2O + Na_2O)] \times 100$; without corrections for apatite and carbonate content (40). We acknowledge that Zr is an imperfect tracer of chemical weathering, due in part to eolian deposition (17, 41, 42) and potential mobility (43, 44), given the high mean annual precipitation in the western Southern Alps (Fig. S5), but argue that it provides first-order constraints on chemical depletion; which is supported by the overall trend of increasing CDF values with increasing CIA values (Fig. S6).

Interpretation of ^{10}Be concentrations

The ^{10}Be concentration in quartz grains within a soil provides an estimate of the soil production rate (i.e., the total denudation rate, or the sum of physical and chemical denudation) at that site, provided the soil is vertically well-mixed (45, 46). We tested the assumption of well-mixed soil with the Alex Knob Pit 4 samples. The soil ^{10}Be concentrations for different depth intervals indicate the soil is well-mixed (Fig. S4). Few studies have evaluated whether soils are vertically-well mixed, but our results are consistent with those expected from bioturbation, as observed in other landscapes (47-49).

Interpretation of ^{10}Be concentrations in soil and sediment as denudation rates requires the assumption of isotopic steady-state, such that the in-going and out-going ^{10}Be flux from a soil profile or watershed is constant over time (45, 49-51). Landslides, which are common in the western Southern Alps (10), have the potential to upset the ^{10}Be balance at both the soil profile and watershed scales. For example, sampling a surface immediately after a landslide removed 1 m of rock would cause erosion rates to be over-estimated by about a factor of three (52). Given the rapid denudation rates in the western Southern Alps, it is not feasible to use a second nuclide, such as ^{26}Al , to test the isotopic steady-state assumption (51), so we carefully selected sampling sites in order to minimize the likelihood of violating the steady-state assumption.

At the soil profile scale, landslides can expose bedrock shielded from cosmic rays, resulting in low ^{10}Be concentrations that are out of equilibrium with long term soil production rates (51, 52). Measuring ^{10}Be concentrations in soils formed on recent landslide scars would result in over-estimation of soil production rates. The time (t) required to return to isotopic equilibrium declines with increasing denudation rate (51) following:

$$t = \frac{\Lambda}{\rho \cdot D} \quad (\text{eq. S1})$$

where Λ is the attenuation length for ^{10}Be production below the surface (160 g cm^{-2}), ρ is rock density, (2.65 g cm^{-3}) and D is the denudation rate (cm yr^{-1}). For example, for a soil production rate of 2 mm yr^{-1} , isotopic equilibrium will be re-established 300 yr following a landslide.

We carefully selected sampling sites to avoid areas with evidence of landsliding. We limited our sampling to convex ridgetops (Fig. S2, S3) where chronic, biogenic disturbance-driven geomorphic processes dominate (53) and avoided planar, threshold hillslopes where episodic landslides are the dominant erosion mechanism (28, 54). Previous work on spatial patterns of vegetation and soils in the western Southern Alps indicates ridges are the most stable portions of the landscape with respect to disturbance by landsliding (55, 56). While in the field we did not observe scars of any recent landslides that breached topographic divides and lowered ridgetop elevations, although we did observe recent landslide scars downslope from ridges. The landslides we did observe resulted in distinct topographic depressions, as even “shallow” landslides erode into bedrock, given the dm-scale soil depths in the western Southern Alps (57). We observed no similar topographic depressions on the ridgetops we sampled, indicating that the landslide return interval for ridgetops is likely to be much longer than those reported for the landscape as a whole. The mean time between landslides (return interval) for a given point on the landscape in the western Southern Alps has been estimated to be both 2,100–15,000 yr (25) and ~ 300 yr (15). Note that the different landslide return intervals are based on the same landslide mapping data (10), but the authors make different assumptions about the continuity (or dis-continuity) of landslide area-frequency distributions; the 2,100–15,000 yr estimate is based directly on the mapped landslide distribution. It is worth noting that both landslide return interval estimates (which likely overestimate landslide frequency on ridgetops) are sufficiently long that ^{10}Be equilibrium can be re-established between landslides for the high soil production rates we measure. In the case where earthquakes on the Alpine Fault caused co-seismic shaking and ridgetop landsliding, as observed following the Chi-Chi earthquake in Taiwan (58), a soil production rate of 2 mm yr^{-1} would be sufficiently rapid to establish a new ^{10}Be equilibrium in the time interval since the most recent ($M_w > 7.6$; 1717 A.D.) earthquake (59). Moreover, none of our ^{10}Be concentrations are consistent with coseismic landsliding during the most recent Alpine Fault rupture—the apparent exposure ages are too old (Table S2). If the soil ^{10}Be data were alternatively interpreted as soil exposure ages that yield information on the time since the last landslide, a soil production rate can be determined by dividing the soil depth by the soil age. For this method to yield true soil production rates, it must be assumed that no erosion of soils formed *in-situ* on the landslide scar has occurred. Such an approach would yield lower soil production rates than those calculated by interpreting the ^{10}Be data as steady-state soil production rates. However, given the steep slope gradients at most of our sampling sites (Table S3), the assumption of no erosion is implausible, hence interpreting soil ^{10}Be concentrations as exposure ages would underestimate soil production rates.

Tree throw is an episodic driver of soil production (60-62) that could also cause ^{10}Be concentrations to be out of steady-state. We explored the potential influence of tree throw on soil production rates with a model similar to those developed to assess potential

errors in denudation rates caused by sampling bedrock surfaces following spallation of a slab of rock (52, 63). We do not attempt to simulate biotic-geomorphic interactions at our field sites, as has been done at other sites with more complete data on vegetation characteristics (62), but use the model results to assess whether the measured ^{10}Be concentrations can reasonably be interpreted as denudation rates. Here we assume that tree throw removes rock from the soil-bedrock interface in a manner analogous to episodic erosion of an outcrop and track the ^{10}Be concentration at the soil-bedrock interface. The model does not simulate mixing of detached material with overlying soil and we assume our results reflect maximum estimates of potential errors, as incorporation of rock transported by tree-throw into a well-mixed regolith would provide additional buffering that minimizes temporal variation of ^{10}Be concentrations in soil. The model also assumes that all denudation is due to physical erosion, which also requires interpreting the error estimates as maximum values. The model uses a finite-difference approach with an annual time-step; the initial condition is a steady state erosion rate, after which erosion becomes unsteady, with periods of no erosion punctuated by periodic removal of a rock slab with a specified thickness. We modeled soil production rate scenarios of 1 mm yr^{-1} and a 2.5 mm yr^{-1} , as we were most concerned with potential over-estimation of higher soil production rates. There are two 1 mm yr^{-1} cases, one in which 100 mm of rock is removed once per century and one in which 300 mm is removed once every 300 yr. There are also two 2.5 mm yr^{-1} cases, one in which 250 mm is eroded once per century and one in which 750 mm is removed once every three centuries.

The modeling results show that, after reaching steady-state, the range of erosion rates interpreted from ^{10}Be in the 1 mm yr^{-1} scenario is $0.93\text{--}1.09 \text{ mm yr}^{-1}$ for the case in which all the erosion occurs once per century and $0.79\text{--}1.29 \text{ mm yr}^{-1}$ for the case in which all the erosion occurs once every three centuries (Fig. S7). One of our measured soil production rates is $1.00\pm 0.08 \text{ mm yr}^{-1}$ and the true uncertainty is likely greater due to uncertainty in ^{10}Be production rate scaling (64, 65). Hence uncertainty in soil production rates predicted by our 1 mm yr^{-1} un-steady erosion rate models is of comparable magnitude to analytical and production rate uncertainty.

The range of erosion rates interpreted from ^{10}Be in the 2.5 mm yr^{-1} scenarios are $2.05\text{--}3.11 \text{ mm yr}^{-1}$ for the case in which all the erosion occurs once per century, which is very similar to the uncertainty in one of our measured values of the same magnitude ($2.47\pm 0.43 \text{ mm yr}^{-1}$). The range of inferred erosion rates for the 2.5 mm yr^{-1} scenario in which all erosion occurs every 300 years is 1.43 to 4.94 mm yr^{-1} (Fig. S7). The magnitude of the erosion (750 mm) is unrealistically high for a single tree fall event, especially given that shrubs are the dominant vegetation at the ridgetops we sampled. Hence, the potential error modeled by this scenario is more representative of error caused by shallow landsliding, which we minimized with our sampling scheme, as described above.

Additionally, whereas the soil production rates we measure in the western Southern Alps are substantially higher than those determined elsewhere using *in situ*-produced ^{10}Be , they are consistent with values estimated using other methods. For example, meteoric ^{10}Be has been used to infer a soil production function in with a y-intercept of 2.1 mm yr^{-1}

for very weak shale bedrock (66). Similarly, soil on anthropogenically-produced bedrock exposures has been shown to form at rates of 5–10 mm yr⁻¹ (given the volume change associated with rock-soil conversion, the equivalent bedrock lowering rates would be about half these values) on sandstone and shale bedrock (67). These two examples highlight the role weak lithology plays in driving rapid soil production rates, and we expect climate and biotic activity to play similar roles in driving high soil production rates in the western Southern Alps.

At the catchment scale, landslides stochastically deliver sediment to channels. The ¹⁰Be concentration in landslide-derived sediment varies with landslide depth. Unless sediment is sufficiently well-mixed such that the ¹⁰Be concentration in sediment transported past the sediment sampling point is steady, the ¹⁰Be concentrations will not accurately represent the true denudation rate (68, 69). The catchment scale at which ¹⁰Be in sediment can be used reliably to infer the denudation rates of the upstream watershed has been modeled to be on the order of 70–100 km² (68, 69). The large catchments we sampled that drain from the Main Divide to the Alpine Fault have areas of 340–450 km², which are sufficiently large to expect steady ¹⁰Be flux. ¹⁰Be disequilibrium is expected to be more likely at small catchment areas, typically resulting in overestimation of denudation rates (68). Denudation rates for the two small (1.6 km²; 12.6 km²) catchments nested within larger catchments are within 1σ error or lower than denudation rates for the larger catchments, and hence do not exhibit evidence of isotopic disequilibrium. The lack of disequilibrium is likely due to the high rates of landsliding in the western Southern Alps, as rivers are always transporting sediment derived from a range of landslide depths. Additionally, though it is not evidence of erosional steady state, we do note that the catchment-scale denudation rates are generally consistent with erosion and exhumation rates averaged over a range of timescales (9-11, 70).

CRONUS calculator inputs and denudation rate calculations

We used the CRONUS calculator (71) to calculate denudation rates (Table S1, S2) from our ¹⁰Be concentrations. The theoretical framework that the CRONUS calculator uses to calculate denudation rates is identical whether the sample is bedrock collected from an outcrop, stream sediment, or vertically-mixed soil (45). To maintain consistency with other studies, we use the ¹⁰Be production rate calibration data encoded in the CRONUS calculator, which are from a wide-range of global sites, in determining denudation rates. More recent calibration efforts from the eastern Southern Alps of New Zealand (65) has resulted in a ¹⁰Be production rate estimate that is ~14% lower than those in the version of the CRONUS calculator we used (Wrapper script v.2.2; Main calculator v.2.1; Objective function v.2; Constants v.2.2.1; Muons v.1.1). Adopting the more proximal calibration data would result in roughly a 14% reduction in the denudation rates we report. Because ¹⁰Be production rate calibration schemes will continue to be improved upon, we report our results and the data required to reproduce our denudation rates in Tables S1-S7. The 1-standard error uncertainties in the denudation rates calculated using the CRONUS calculator include errors in the number of ⁹Be atoms added to each sample, errors in the ¹⁰Be concentration of procedural and carrier blanks, and errors in the AMS isotope ratio measurements, added in quadrature.

We calculated catchment-averaged ^{10}Be production rate scaling factors by determining production rates for each grid cell in a DEM, using the elevation and latitude of each grid cell, as described by Greg Balco (http://depts.washington.edu/cosmolab/P_by_GIS.html). We used production rate scaling factors to calculate the elevation input for the CRONUS calculator, using the mean catchment latitude and Lal's polynomial ^{10}Be production rate scaling scheme (51). The catchment-averaged production rates we use assume zero ^{10}Be production for the portions of each catchment with permanent snow and ice cover (11%, 13%, and 4% of the Karangarua, Whataroa, and Hokitika catchments, respectively), using 1:50,000 scale data from Land Information New Zealand (<http://data.linz.govt.nz/layer/352-nz-mainland-snow-polygons-topo-150k/>). The thickness of all soil and sediment samples was set to an arbitrarily low value of 0.1 cm, as the ^{10}Be concentration at the surface is the relevant value for determining denudation rates in both vertically-mixed soils and sediment (45). The density values are mean values from multiple bedrock samples from each soil pit; catchment bedrock density values are the mean value of all soil pit samples within the watershed.

Topographic shielding of soil pits was calculated based on the hillslope angle of the sample site. The thick vegetation in the western Southern Alps generally blocked our view of the horizon, so we did not collect data for determining a shielding correction due to distant topography. Given our samples were from ridgetops, distant topography is expected to cause little shielding. We were able to climb on top of the single bedrock outcrop we sampled, which did afford a view of the horizon. The shielding factor determined for distant topography at this site is extremely small (0.999), indicating that by neglecting to account for shielding from distant topography, we are introducing very small errors that are orders of magnitude lower than the AMS measurement uncertainty. We calculated catchment-scale topographic shielding factors by first assuming that cosmic rays are conserved, such that all cosmic rays that enter a catchment produce ^{10}Be within the catchment. We then assumed that all cosmic rays entering a catchment pass through a plane that projects from the catchment outlet to the maximum catchment elevation. The angle of the catchment surface plane was then used to determine catchment scale shielding factors in a manner analogous to determining the shielding factor for a sample on a sloping surface (72). The denudation rates we report in Tables S2 and S4 are based on time-dependent ^{10}Be production and the Lal-Stone (51, 73) latitude and altitude scaling scheme.

Quartz is resistant to dissolution; hence the mean residence time for quartz in soils is longer than the mean residence time of all minerals (74). The enrichment of quartz biases denudation rate estimates (75). We corrected our soil denudation rate measurements for quartz enrichment by assuming Zr is similarly enriched in our samples (74, 75). The chemical erosion factors (CEF) are generally small, with an average of 1.06 (Table S3). For all corrections we assume a soil density of 1.0 g cm^{-3} (approximately the mean of the measured values (76)) and an attenuation length of 160 g cm^{-2} .

Chemical weathering

Soil and bedrock Zr concentrations were used to determine chemical depletion fractions (*CDF*), where:

$$CDF = \left(1 - \frac{[Zr]_{rock}}{[Zr]_{soil}} \right) \quad (\text{eq. S2})$$

which is equivalent to the ratio of chemical denudation to total denudation (18, 38). Hence chemical denudation (W) can be determined:

$$W = D \cdot \left(1 - \frac{[Zr]_{rock}}{[Zr]_{soil}} \right) \quad (\text{eq. S3})$$

where D is the soil production or total denudation rate. Since:

$$D = W + E \quad (\text{eq. S4})$$

and E is the physical denudation rate, E can be determined from D and W . Errors in D were propagated in calculating W and E . Bedrock Zr was measured in a composite sample consisting of one or more pieces of bedrock from the base of each pit. Similarly, soil Zr was measured in a split of a large, homogenized sample that included rock fragments; hence we assume these data represent mean Zr concentrations. Because measurement errors in the Zr data are small (± 2 ppm) relative to the concentrations we measured (Table S3), and are not expected to vary among samples, we did not propagate Zr measurement error in our calculations of W .

World-wide soil production function, physical denudation, and chemical denudation data

The soil production functions in Fig. 2b are compiled from refs. 16, 22, 60, 77-82. The soil production functions are as originally published; for example, no corrections have been made for updates of ^{10}Be production rate scaling.

The soil physical and chemical denudation rate data in Fig. 3 are compiled from refs. 17, 18, 39, 83-86. The physical and chemical denudation data are as originally published, except some of those from ref. 18, which have been re-calculated using chemical erosion factors reported in ref. 87. The catchment-based physical and chemical denudation rate data are for 299 ocean-draining rivers from ref. 29. Pre-dam denudation data were used when these data were reported and data from five rivers in the database (Colorado, Haihe, Rhine, Patuxent, and Severn) were excluded from the statistical analyses due to high anthropogenic influence on either chemical or physical denudation; other rivers in the dataset have, of course, been impacted by humans and a full description of the data is available in ref. 29. Removal of five rivers resulted in an increase in the R^2 value of the chemical-physical denudation regression relationship, but had very little influence on the power-law scaling exponent. The chemical denudation data from the western Southern Alps are from refs. 12 and 30, whereas the physical denudation data are updated suspended sediment discharge values from ref. 11. Data are shown only for rivers with measurements; unlike the original publications, no extrapolated values are shown.

Supplementary Text

Study site descriptions

We limited our sampling to sites near (or directly on) the ridgecrest because the ridge-tops lacked morphologic evidence for recent landsliding, and are hence more likely to be in steady-state with respect to ^{10}Be and soil thickness, as described above. Topographic data are not available for our sites at a resolution suitable for calculating quantitative metrics of hillslope morphology, but the ridges are convex landforms with local-scale topographic heterogeneity. Qualitatively, the overall ridge curvature varied among the sites; the ridge at Rapid Creek site was sharply convex and the ridge-top was only a few m wide in some areas, in contrast to the broader tens of meters wide ridge-tops at the other sites, which may explain the higher soil production rates at the Rapid Creek site (88, 89). The ridges are not smooth over length scales greater than ~ 10 m, which differs from many sites where soil production rates have been measured previously and morphology is more consistent with the assumption of steady-state soil thickness (16). Some of the local-scale topographic variability may arise from tree-throw, though the shrubs that were the dominant vegetation at many of the sample locations are not likely to generate well-developed pit-and-mound topography; instead the local scale topographic variability is likely a function of the structural heterogeneity of the pervasively jointed and fractured bedrock. Additionally, ridge-top topography throughout the Southern Alps is influenced by gravitational collapse of bedrock, generating ridge rents or sackung (90), which we suggest also contributes to local-scale topographic variability. At the Karangarua site, we observed offset in bedrock consistent with gravitational collapse. Areas adjacent to the Karangarua and Gunn Ridge sites have been identified as areas that contain or are suspected to contain deep-seated gravitational failures (91) and the gravitational collapse may extend spatially beyond the mapped failures to the sites we sampled and contribute to the non-smooth character of the ridges. We did not observe evidence of gravitational failure at the Fox, Alex Knob, and Rapid Creek sites.

Soil production rates have been previously measured at sites with locally variable topography and the potential for stochastic erosion process via careful site selection (22, 60). Because slopes were not smooth, we did not sample in straight, down-slope transects, but carefully selected sites to avoid areas with evidence for past disturbance or disequilibrium. The soil morphology in each pit was examined prior to sampling. Soils exhibiting evidence of truncation or burial (e.g., buried horizons, multiple hardpans) were not sampled and the soils we did collect had well-developed organic horizons and exhibited well-developed root systems. Our primary objective in sampling was to select soils that spanned a range of soil thicknesses and did not exhibit evidence of non-steady soil thickness. We observed few areas where soil thickness was < 10 cm, save scattered bedrock outcrops standing high above the soil surface. We note that we measured ^{10}Be concentration in quartz separated from soil, rather than underlying bedrock, which is a different approach than most previous soil production rate studies (16, 22, 60, 77-82), as this method does not require a cosmic ray shielding correction based on an assumption of steady-state soil thickness. Although the assumption of steady-state soil thickness is required to determine soil production functions (the regression relationship between soil production rate and soil thickness), the denudation rates we measure do not depend on

this assumption and are robust, providing that soils are vertically-mixed (45, 46). Whereas it is difficult, if not impossible to strictly test the assumption of steady soil thickness, the assumption of vertically-mixed soils can be tested with samples collected from multiple depth intervals, and data from Alex Knob Pit 4 indicate the soils we sampled are vertically mixed. Only the Karangarua, Gunn Ridge, and Rapid Creek sites have enough samples ($n \geq 5$) to define soil production functions. The Gunn Ridge and Rapid Creek sites exhibit well-defined soil production functions, consistent with the interpretation that the soils we sampled are in steady-state with respect to soil thickness. However, the Karangarua site does not exhibit an exponential decline in soil production rate with increasing soil thickness, suggesting that the soil depths and ^{10}Be concentrations rates for some of the soils we sampled may not be in equilibrium. The principle outlier from the Karangarua site (Pit 3) is a thin soil (15 cm) with an extremely low CDF of 0.01. In a landscape with episodically driven erosion, it might be expected that the thin, unweathered soil formed on bedrock exposed by a recent mass failure and would yield an unreasonably high denudation rate. However, the denudation rate is quite low and similar to the bedrock outcrop we sampled at this site, suggesting this area, which was the highest elevation sampled at the Karangarua site, may have been exposed bedrock or grassy, tussock vegetation that has more recently been colonized by shrub vegetation, given the lower bioturbation erosion efficiency of grassland vegetation (92).

Landsliding results in a landscape with surfaces of varying age and geochemical development. If the pattern of landsliding is heterogeneous in space, then a watershed may maintain a geochemical quasi-steady state, despite the episodic nature of landslide triggering. In the western Southern Alps, landslides are distributed relatively evenly between valley bottoms and ridges (58), suggesting landsliding is spatially heterogeneous, at least with respect to elevation.



Fig. S1.

Photos of roots penetrating bedrock exposed by a recent tree fall. **(A)** Coarse (cm-scale) roots growing in a foliation plane have opened an 8–10 cm fracture and have broken off a ~10 cm thick slab of schist. **(B)** Fine (mm-scale) roots growing within planes of weakness within the schist contribute to chemical weathering and can physically spall mm-thick pieces of bedrock.

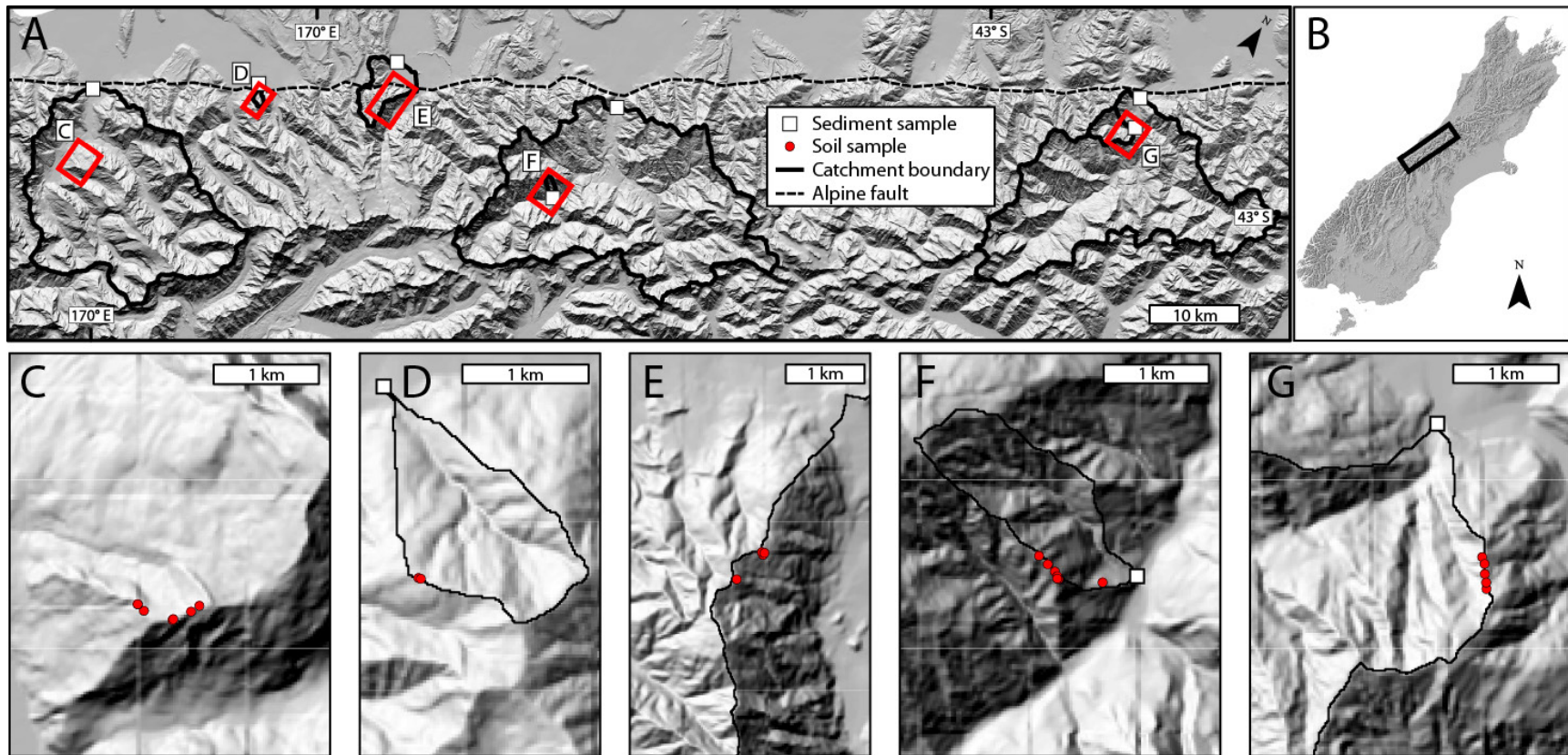


Fig. S2.

Sample locations. (A) Hillshade map of the study area. The red boxes outline the bounds of panels C–G. (B) Location of the study area on New Zealand’s South Island. Locations of soil samples on ridgetops at the Karangarua (C), Fox (D), Alex Knob (E), Gunn Ridge (F), and Rapid Creek (G) study sites. Note that the map in panel A is the same as Figure 1, which contains denudation rate results.

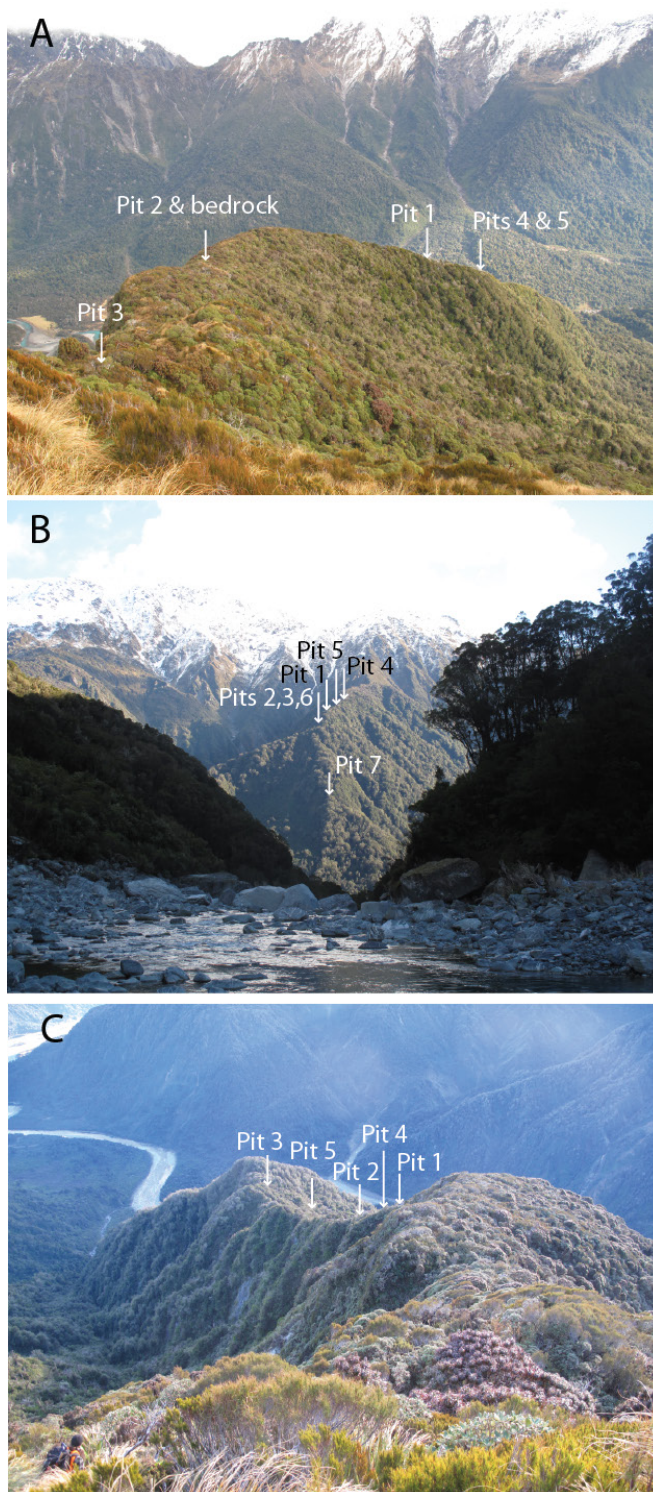


Fig. S3.

Photos of the ridges sampled in the (A) Karangarua, (B) Whataroa, and (C) Hokitika catchments. The arrows show the approximate location of the sample sites. Note that the dense vegetation is rooted in a near-continuous soil mantle.

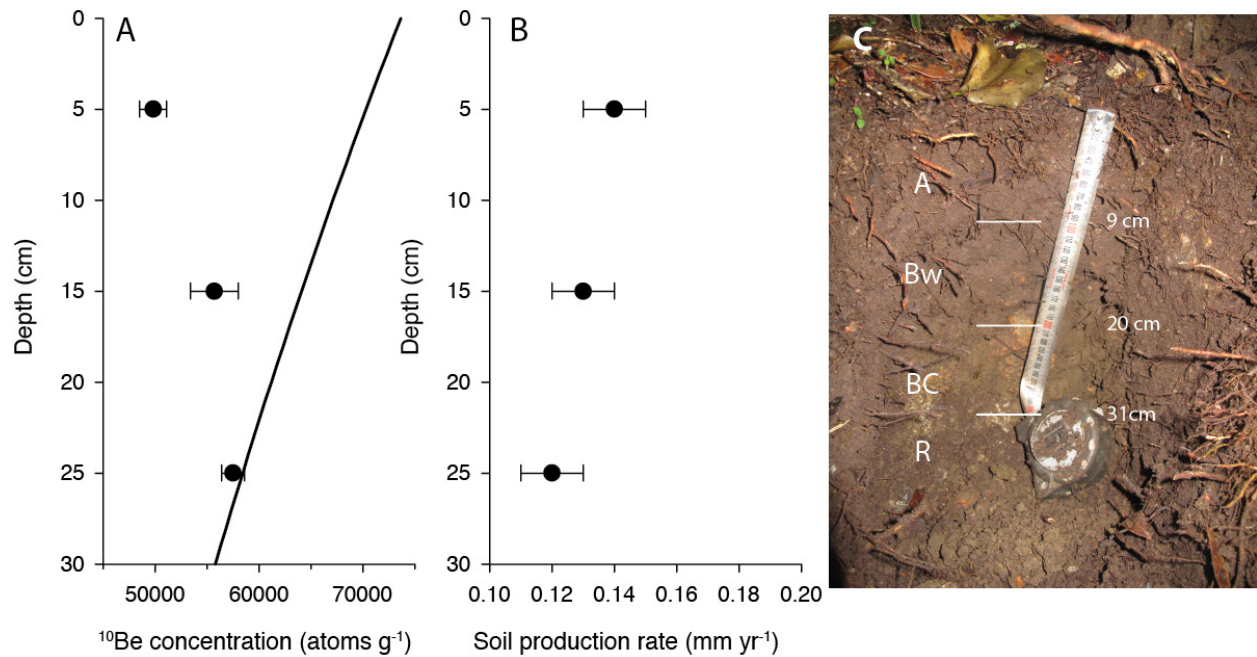


Fig. S4.

Alex Knob Pit 4 soil depth profile. **(A)** ^{10}Be concentrations for samples from three depths. The upper, middle, and lower samples span the 0–10 cm, 10–20 cm, and 20–30 cm depths, respectively. The black curve is the predicted ^{10}Be concentration for an unmixed soil, using a bulk density of 1.48 g cm^{-3} , the mean for the mineral Bw and BC horizons. The data do not follow the trend predicted by no mixing, indicating the soil has been mixed vertically by bioturbation. Error bars indicate 1 standard error. **(B)** Soil production rates inferred from the ^{10}Be concentrations. **(C)** Photo of the soil with designated soil horizons. The soil horizons correspond closely (within 1 cm) to the sample depth increments. Munsell color of horizons: A: 10YR 2/2; Bw: 10YR 3/2.5; BC: 2.5Y 4/2-3.

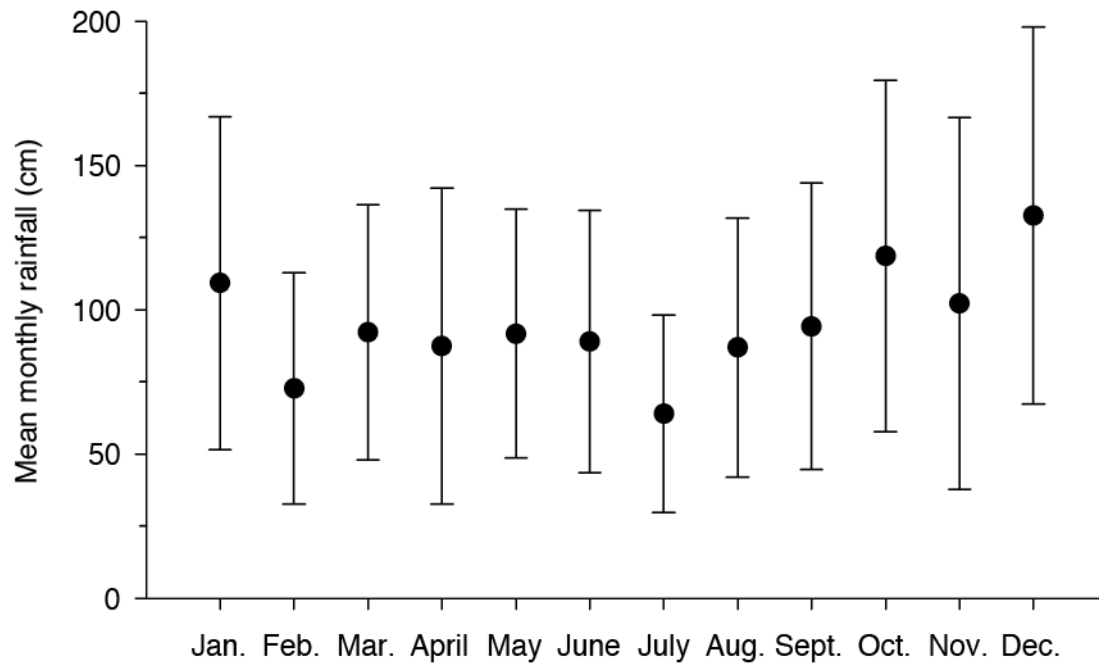


Fig. S5.

Mean and standard deviation of monthly rainfall at the Cropp at Waterfall rain gage. The rain gage is in the Cropp River catchment, which is adjacent to the Rapid Creek catchment we sampled, at an elevation of 975 m. The mean annual precipitation at this site is 11.52 m. Data are from July 1982 to October 2012, courtesy of the New Zealand National Institute of Water and Atmospheric Research. The mean annual temperature is approximately 5.5 °C (ref. 14).

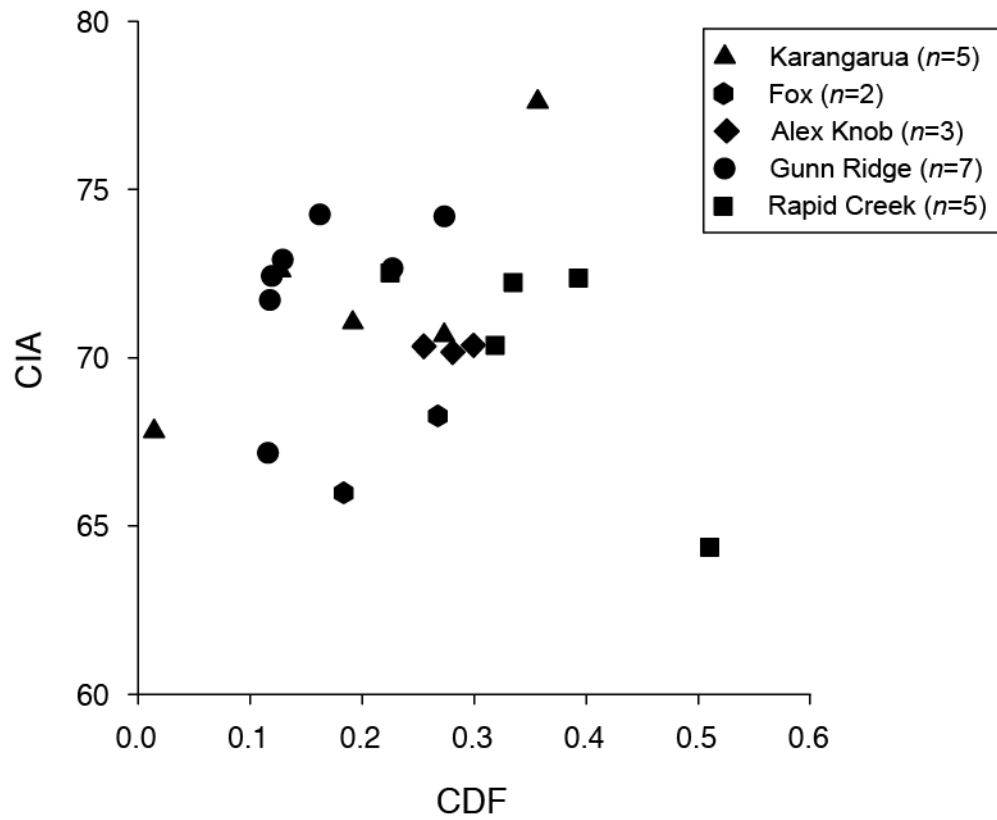


Fig. S6.

Chemical Index of Alteration (CIA) versus CDF values for soils from the Western Southern Alps. The two, independent weathering indices generally increase with one another (although one of the Rapid Creek sites is an outlier), suggesting that Zr-based CDF values provide a first order view of the degree of chemical weathering at our study sites.

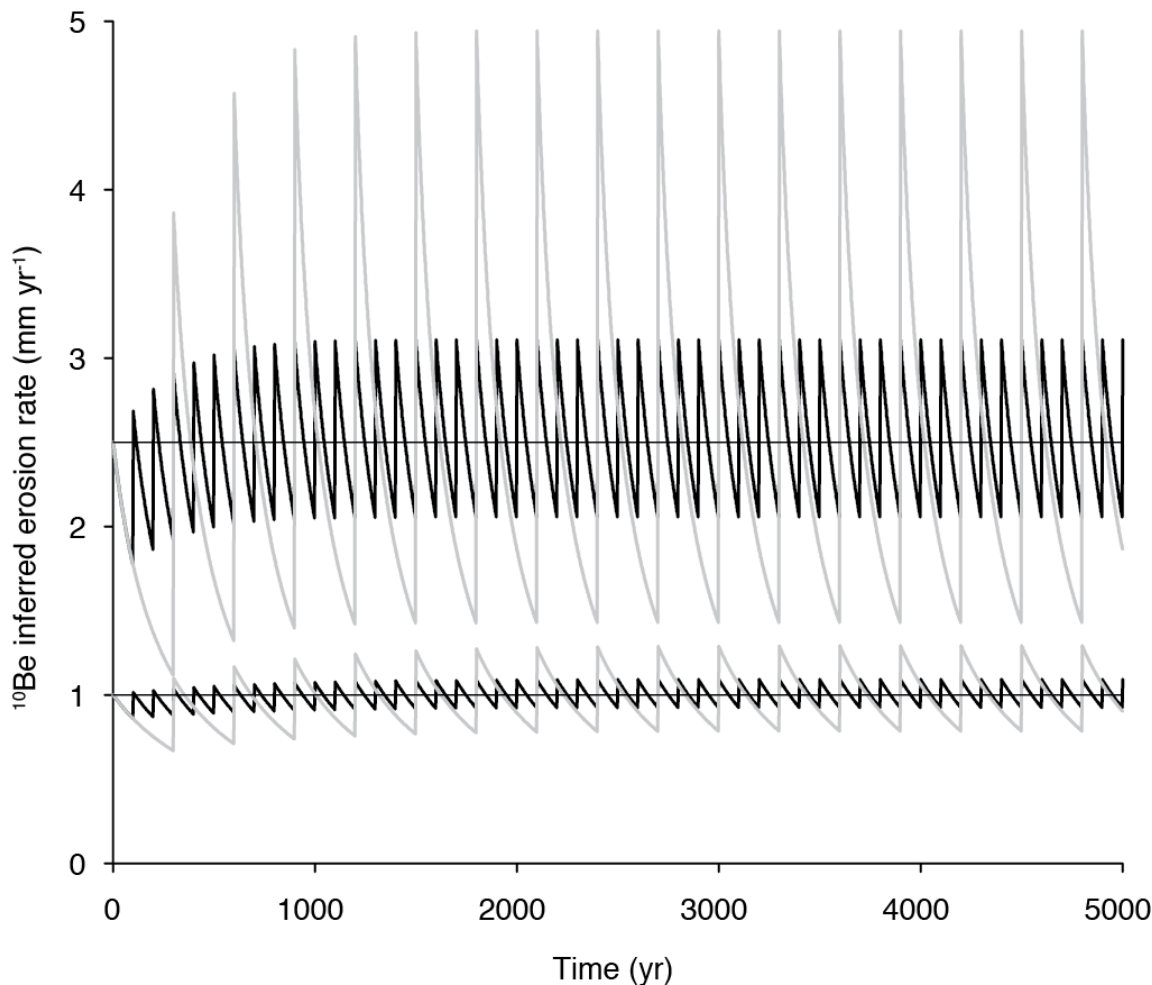


Fig. S7.

Variability in inferred soil production rates due to unsteady erosion. The upper and lower sets of curves are for 2.5 mm yr^{-1} and 1 mm yr^{-1} soil production rate scenarios, respectively. For both scenarios, the thin, horizontal black line shows steady soil production, the thick black line shows soil production rates inferred from ^{10}Be when all erosion occurs once per century, and the gray line shows soil production rates inferred from ^{10}Be when all erosion occurs once every three centuries. The variability in inferred soil production rates caused by unsteady erosion is of the same (or lower) magnitude than analytical and ^{10}Be production rate scaling uncertainty, except for the 2.5 mm yr^{-1} scenario where all erosion occurs once every 300 yr. In this case, the 750 mm of erosion is unrealistically high for a single tree fall event, but comparable to what might be expected due to shallow landsliding. As explained in the text, we designed our sampling strategy to avoid sampling areas subject to recent landsliding.

Table S1.

CRONUS calculator inputs. All samples assume a standard atmosphere and are normalized to the 07KNSTD ^{10}Be standard. The input sample thickness is 0.1 cm for all samples, with the exception of the Karangarua bedrock outcrop sample, which had a thickness of 1.6 cm. Sample location coordinates are reported in Table S7.

Sample name	Lat.	Lon.	Elev. (m)	Density (g cm^{-3})	Shielding factor	^{10}Be conc. (atom g^{-1})	^{10}Be conc. uncertainty (atom g^{-1})
Karangarua-Pit-1	-43.6485	169.8466	1030	2.73	0.9889	28100	1300
Karangarua-Pit-2	-43.6493	169.8499	1082	2.60	0.9819	57000	2300
Karangarua-Pit-3	-43.6486	169.8521	1112	2.74	0.9564	73800	1600
Karangarua-Pit-4	-43.6480	169.8458	959	2.73	0.9797	20840	590
Karangarua-Pit-5	-43.6479	169.8458	961	2.72	0.9260	24800	1000
Karangarua-bedrock	-43.6493	169.8500	1085	2.74	0.9988	66000	2500
Karangarua-sed	-43.6500	169.9260	1004	2.70	0.9998	2220	180
Fox-Pit-1	-43.4943	169.9984	932	2.66	0.9874	35200	900
Fox-Pit-2	-43.4944	169.9986	942	2.65	0.9839	70600	1300
Fox_sed	-43.4906	170.0040	731	2.66	0.9874	4800	430
Alex-Knob-Pit-2	-43.4168	170.1574	846	2.68	0.9600	48700	1100
Alex-Knob-Pit-3	-43.4199	170.1534	947	2.69	0.9633	43000	1500
Alex_Knob_Pit_4_0-10_cm	-43.4169	170.1577	836	2.70	0.9874	49800	1300
Alex_Knob_Pit_4_10-20_cm	-43.4169	170.1577	836	2.70	0.9874	55700	2300
Alex_Knob_Pit_4_20-30_cm	-43.4169	170.1577	836	2.70	0.9874	57500	1100
Docherty_Creek_sed	-43.4102	170.1380	562	2.69	0.9985	2840	180
Gunn-Pit-1	-43.4040	170.4046	866	2.73	0.9874	14440	680
Gunn_Pit_2	-43.4047	170.4050	832	2.66	0.9723	20080	830
Gunn-Pit-3	-43.4044	170.4048	856	2.57	0.9446	19530	770
Gunn_Pit_4	-43.4027	170.4027	953	2.70	0.9857	43600	1900
Gunn-Pit-5	-43.4034	170.4037	910	2.65	0.9874	30400	1500
Gunn-Pit-6	-43.4046	170.4048	838	2.65	0.9750	20300	800
Gunn-Pit-7	-43.4050	170.4102	555	2.67	0.9750	23900	900
Gunn-Ridge-sed	-43.3975	170.4010	944	2.68	0.9819	870	200
Whataroa-sed	-43.3722	170.4890	1017	2.68	0.9998	1260	330
Rapid-Creek-Pit-1	-43.0294	171.0175	966	2.97	0.9633	24900	1100
Rapid-Creek-Pit-2	-43.0282	171.0173	897	2.61	0.9260	11100	560
Rapid-Creek-Pit-3	-43.0267	171.0170	856	2.59	1.0000	8020	330
Rapid-Creek-Pit-4	-43.0289	171.0175	946	2.59	0.8916	3160	500
Rapid-Creek-Pit-5	-43.0273	171.0173	832	2.65	0.9819	6830	340
Rapid-Creek-sed	-43.0308	170.9860	1070	2.68	0.9948	1640	150
Hokitika_sed	-43.0828	171.0424	1124	2.68	0.9997	760	120

Table S2.

Denudation rate and apparent exposure ages determined using the CRONUS calculator. Note that we do not use the soil denudation rate data presented here in our analyses, but the CEF-corrected values reported in Table S4. Note: 1.0 Mg (megagram) = 1.0 t (tonne) = 1000 kg.

Sample name	Denudation rate (mm yr ⁻¹)	Denudation rate uncertainty (mm yr ⁻¹)	Denudation rate (Mg km ⁻² yr ⁻¹)	Denudation rate uncertainty (Mg km ⁻² yr ⁻¹)	Apparent exposure age (yr)	Apparent exposure age uncertainty (yr)
Karangarua-Pit-1	0.29	0.02	790	60	2650	260
Karangarua-Pit-2	0.15	0.01	400	30	5150	480
Karangarua-Pit-3	0.11	0.01	300	20	6600	580
Karangarua-Pit-4	0.37	0.03	1010	70	2100	190
Karangarua-Pit-5	0.30	0.02	820	60	2630	250
Karangarua-bedrock	0.13	0.01	350	30	5890	550
Karangarua-sed	3.70	0.39	9990	1040	210	30
Fox-Pit-1	0.22	0.02	590	40	3600	320
Fox-Pit-2	0.11	0.01	290	20	7040	610
Fox_sed	1.44	0.16	3840	420	580	70
Alex-Knob-Pit-2	0.15	0.15	390	30	5440	480
Alex-Knob-Pit-3	0.18	0.18	480	40	4420	400
Alex_Knob_Pit_4_0-10_cm	0.14	0.14	390	30	5460	480
Alex_Knob_Pit_4_10-20_cm	0.13	0.13	350	30	6070	570
Alex_Knob_Pit_4_20-30_cm	0.12	0.12	340	20	6260	540
Docherty_Creek_sed	0.15	0.15	5900	520	390	40
Gunn-Pit-1	2.19	0.19	1380	110	1570	150
Gunn_Pit_2	0.51	0.04	960	70	2270	210
Gunn-Pit-3	0.36	0.03	980	70	2220	210
Gunn_Pit_4	0.38	0.03	480	40	4370	420
Gunn-Pit-5	0.18	0.01	670	60	3170	310
Gunn-Pit-6	0.25	0.02	960	70	2270	210
Gunn-Pit-7	0.36	0.03	680	50	3370	310
Gunn-Ridge-sed	0.25	0.02	24200	6100	90	20
Whataroa-sed	9.02	2.26	17700	5100	120	30
Rapid-Creek-Pit-1	0.28	0.02	830	70	2560	240
Rapid-Creek-Pit-2	0.67	0.05	1740	140	1260	120
Rapid-Creek-Pit-3	0.96	0.07	2490	190	870	80
Rapid-Creek-Pit-4	2.38	0.42	6170	1080	360	60
Rapid-Creek-Pit-5	1.07	0.09	2840	230	770	80
Rapid-Creek-sed	5.19	0.59	13900	1600	150	20
Hokitika_sed	11.65	2.04	31200	5500	70	10

Table S3.

Soil loss-on-ignition (LOI), soil and bedrock Zr data, chemical depletion fractions (CDF), and chemical erosion factor (CEF) correction for quartz enrichment in soil (74, 75, 89), soil depth, and soil sampling site slope data. Note that the CEF used here is equivalent to the quartz dissolution factor (C_d) of ref. 75, where Zr enrichment in soil is used as a proxy for quartz enrichment. Saprolite weathering is assumed to be minimal in the CEF calculations (89).

Sample name	Soil LOI (%)	Zr _{soil} (ppm)	LOI _{corrected} Zr _{soil} (ppm)	Zr _{rock} (ppm)	CDF	CEF	Soil thickness (cm)	Local slope (degrees)
Karangarua-Pit-1	3.9	237	246	199	0.19	1.05	40	24
Karangarua-Pit-2	15.0	288	331	213	0.36	1.07	21	28
Karangarua-Pit-3	2.6	259	266	262	0.01	1.00	15	37
Karangarua-Pit-4	5.8	209	221	193	0.13	1.02	21	29
Karangarua-Pit-5	10.9	330	366	266	0.27	1.02	10	44
Fox-Pit-1	13.4	255	289	236	0.18	1.04	32	25
Fox-Pit-2	12.2	275	309	226	0.27	1.04	20	27
Alex-Knob-Pit-2	8.8	257	280	201	0.28	1.09	41	36
Alex-Knob-Pit-3	5.7	289	305	214	0.30	1.04	15	35
Alex_Knob_Pit_4_0-10_cm	8.5	224	243	181	0.26	1.06	31	29
Alex_Knob_Pit_4_10-20_cm	6.9	260	278	181	0.35	1.09	31	29
Alex_Knob_Pit_4_20-30_cm	5.5	215	227	181	0.20	1.04	31	29
Gunn-Pit-1	12.7	220	248	219	0.12	1.02	24	25
Gunn_Pit_2	7.6	238	256	223	0.13	1.02	25	32
Gunn-Pit-3	6.0	256	271	239	0.12	1.02	29	40
Gunn_Pit_4	8.2	262	284	206	0.27	1.08	39	26
Gunn-Pit-5	9.9	226	248	219	0.12	1.02	30	25
Gunn-Pit-6	6.0	243	258	199	0.23	1.05	27	31
Gunn-Pit-7	10.8	208	230	193	0.16	1.04	34	31
Rapid-Creek-Pit-1	5.1	208	219	107	0.51	1.23	40	35
Rapid-Creek-Pit-2	10.1	253	279	169	0.39	1.11	30	44
Rapid-Creek-Pit-3	7.1	233	249	170	0.32	1.04	16	0
Rapid-Creek-Pit-4	6.8	221	236	157	0.33	1.04	12	50
Rapid-Creek-Pit-5	25.4	213	267	207	0.23	1.03	15	28

Table S4.

CEF-corrected soil denudation rate data. T = total denudation (soil production) rate, W = chemical denudation rate, and E = physical denudation rate.

Sample name	T (mm yr ⁻¹)	±T (mm yr ⁻¹)	T (Mg km ⁻² yr ⁻¹)	±T (Mg km ⁻² yr ⁻¹)	W (mm yr ⁻¹)	±W (mm yr ⁻¹)	W (Mg km ⁻² yr ⁻¹)	±W (Mg km ⁻² yr ⁻¹)	E (mm yr ⁻¹)	±E (mm yr ⁻¹)	E (Mg km ⁻² yr ⁻¹)	±E (Mg km ⁻² yr ⁻¹)
Karangarua-Pit-1	0.30	0.02	830	70	0.056	0.005	150	10	0.25	0.02	680	70
Karangarua-Pit-2	0.16	0.01	430	30	0.054	0.005	140	10	0.11	0.01	280	40
Karangarua-Pit-3	0.11	0.01	310	20	0.0016	0.0001	4.4	0.3	0.11	0.01	300	20
Karangarua-Pit-4	0.38	0.03	1030	80	0.047	0.004	130	10	0.33	0.03	900	80
Karangarua-Pit-5	0.31	0.02	830	60	0.082	0.006	220	20	0.22	0.02	610	70
Fox-Pit-1	0.23	0.02	610	40	0.041	0.003	110	10	0.19	0.02	510	40
Fox-Pit-2	0.12	0.01	310	20	0.030	0.002	80	10	0.09	0.01	230	20
Alex-Knob-Pit-2	0.16	0.01	430	30	0.041	0.003	110	10	0.12	0.01	320	30
Alex-Knob-Pit-3	0.18	0.01	500	40	0.053	0.004	140	10	0.13	0.01	350	40
Alex_Knob_Pit_4_0-10_cm	0.15	0.01	410	30	0.037	0.003	100	10	0.12	0.01	310	30
Alex_Knob_Pit_4_10-20_cm	0.14	0.01	380	30	0.045	0.004	120	10	0.10	0.01	260	30
Alex_Knob_Pit_4_20-30_cm	0.13	0.01	350	20	0.025	0.002	70	10	0.11	0.01	280	30
Gunn-Pit-1	0.51	0.04	1410	110	0.059	0.005	160	10	0.46	0.04	1250	110
Gunn_Pit_2	0.37	0.03	980	80	0.047	0.004	120	10	0.32	0.03	860	80
Gunn-Pit-3	0.39	0.03	1000	80	0.046	0.004	120	10	0.34	0.03	890	80
Gunn_Pit_4	0.19	0.02	520	40	0.049	0.004	130	10	0.14	0.02	390	40
Gunn-Pit-5	0.26	0.02	690	60	0.030	0.003	80	10	0.23	0.02	610	60
Gunn-Pit-6	0.38	0.03	1000	80	0.082	0.006	220	20	0.29	0.03	780	80
Gunn-Pit-7	0.26	0.02	700	50	0.041	0.003	110	10	0.22	0.02	590	50
Rapid-Creek-Pit-1	0.34	0.03	1020	80	0.14	0.01	420	40	0.20	0.03	600	90
Rapid-Creek-Pit-2	0.74	0.06	1930	160	0.26	0.02	690	60	0.48	0.06	1250	170
Rapid-Creek-Pit-3	1.00	0.08	2600	200	0.31	0.02	790	60	0.70	0.08	1810	210
Rapid-Creek-Pit-4	2.47	0.43	6390	1110	0.80	0.14	2060	370	1.67	0.45	4330	1180
Rapid-Creek-Pit-5	1.10	0.09	2910	240	0.24	0.02	640	50	0.86	0.09	2270	240

Table S5.

Blank information, sample size, Be carrier weights, isotope ratio, and quartz yield data. ^9Be carrier concentration error=0.8%. na=not applicable. $^{10}\text{Be}/^9\text{Be}$ ratios for samples are corrected for blanks.

Sample name	Blank name	Sample mass (g quartz)	Be carrier (μg)	$^{10}\text{Be}/^9\text{Be}$ ratio	$^{10}\text{Be}/^9\text{Be}$ ratio uncertainty	Quartz yield from bulk soil (%)	Quartz yield from 250-850 μm fraction (%)
Karangarua-Pit-1	Blank_ijkl_15feb2012	31.5248	244.4	5.417E-14	2.43E-15	2.3	35.2
Karangarua-Pit-2	Blank-ijkl31aug2012	20.3623	244.9	7.093E-14	2.85E-15	2.0	32.9
Karangarua-Pit-3	Blank_ijkl_15feb2012	31.5192	244.9	1.421E-13	3.1E-15	2.5	56.1
Karangarua-Pit-4	Blank_ijkl_15june2012	33.2208	244.8	4.232E-14	1.20E-15	3.2	38.2
Karangarua-Pit-5	Blank_ijkl_15feb2012	32.3650	244.5	4.913E-14	1.97E-15	2.4	28.9
Karangarua-bedrock	Blank_ijkl_3aug2012	24.2542	245.8	9.749E-14	3.70E-15	na	37.1
Karangarua-sed	Blank_ijkl_15feb2012	37.4834	244.0	5.102E-15	4.13E-16	na	30.1
Fox-Pit-1	Blank-ijkl31aug2012	25.9308	245.8	5.551E-14	1.38E-15	3.4	17.6
Fox-Pit-2	Blank-ijkl31aug2012	26.8048	246.0	1.152E-13	2.2E-15	5.0	52.1
Fox_sed	Blank_ijkl_3aug2012	38.6035	246.2	1.128E-14	1.00E-15	na	20.7
Alex-Knob-Pit-2	Blank-ijkl31aug2012	24.9813	245.2	7.423E-14	1.66E-15	2.4	39.7
Alex-Knob-Pit-3	Blank-ijkl31aug2012	24.7428	246.0	6.471E-14	2.31E-15	2.6	32.3
Alex_Knob_Pit_4_0-10_cm	Blank_ijkl_3aug2012	27.2564	246.2	8.254E-14	2.21E-15	1.4	23.4
Alex_Knob_Pit_4_10-20_cm	Blank_ijkl_3aug2012	27.3397	246.1	9.254E-14	3.81E-15	1.6	22.8
Alex_Knob_Pit_4_20-30_cm	Blank_ijkl_3aug2012	27.8965	245.9	9.765E-14	1.89E-15	1.3	33.0
Docherty_Creek_sed	Blank_ijkl_3aug2012	37.6864	245.9	6.514E-15	4.17E-16	na	20.5

Table S6.

Blank information, sample size, Be carrier weights, isotope ratio, and quartz yield data. ^9Be carrier concentration error=0.8%. na=not applicable. $^{10}\text{Be}/^9\text{Be}$ ratios for samples are corrected for blanks.

Sample name	Blank name	Sample mass (g quartz)	Be carrier (μg)	$^{10}\text{Be}/^9\text{Be}$ ratio	$^{10}\text{Be}/^9\text{Be}$ ratio uncertainty	Quartz yield from bulk soil (%)	Quartz yield from 250-850 μm fraction (%)
Gunn-Pit-1	Blank_ijl_15june2012	25.5671	244.4	2.260E-14	1.06E-15	1.4	25.4
Gunn_Pit_2	Blank_ijl_3aug2012	28.2016	245.5	3.452E-14	1.42E-15	1.2	32.7
Gunn-Pit-3	Blank_ijl_15june2012	25.8279	244.6	3.086E-14	1.21E-15	1.7	45.2
Gunn_Pit_4	Blank_ijl_15june2012	25.0069	243.8	6.689E-14	2.86E-15	1.6	34.5
Gunn-Pit-5	Blank-205-IL-JS	24.8587	243.6	4.640E-14	2.26E-15	1.8	26.5
Gunn-Pit-6	Blank-ijl31aug2012	24.7996	246.2	3.064E-14	1.14E-15	1.7	46.4
Gunn-Pit-7	Blank-ijl31aug2012	25.7644	245.2	3.757E-14	1.44E-15	1.2	23.5
Gunn-Ridge-sed	Blank-205-IL-JS	33.5699	242.6	1.794E-15	4.04E-16	na	21.7
Whataroa-sed	Blank_ijl_15feb2012	38.2650	242.8	2.966E-15	7.84E-16	na	25.4
Rapid-Creek-Pit-1	Blank_ijl_15june2012	32.3075	244.6	4.917E-14	2.13E-15	1.9	35.0
Rapid-Creek-Pit-2	Blank_ijl_15june2012	29.0639	244.8	1.972E-14	9.90E-16	2.7	14.0
Rapid-Creek-Pit-3	Blank_ijl_15feb2012	30.5438	245.1	1.496E-14	6.2E-16	2.2	23.5
Rapid-Creek-Pit-4	Blank_ijl_15june2012	31.0972	244.8	6.008E-15	9.40E-16	1.6	18.2
Rapid-Creek-Pit-5	Blank-ijl31aug2012	30.1100	245.4	1.254E-14	6.2E-16	2.1	18.4
Rapid-Creek-sed	Blank_ijl_15feb2012	37.2632	244.7	3.739E-15	3.51E-16	na	20.4
Hokitika_sed	Blank_ijl_3aug2012	37.8328	245.8	1.741E-15	2.78E-16	na	20.0
Blank_ijl_15feb2012	Blank_ijl_15feb2012	na	244.5	4.782E-16	1.183E-16	na	na
Blank_ijl_15june2012	Blank_ijl_15june2012	na	244.8	1.030E-15	6.22E-16	na	na
Blank_ijl_3aug2012	Blank_ijl_3aug2012	na	246.1	5.361E-16	1.169E-16	na	na
Blank-205-IL-JS	Blank-205-IL-JS	na	242.1	2.947E-16	2.214E-16	na	na
Blank-ijl31aug2012	Blank-ijl31aug2012	na	245.4	4.489E-16	2.964E-16	na	na

Table S7.

Sample locations. UTM zone 59S, WGS84 datum.

Sample name	Northing (m)	Easting (m)
Karangarua-Pit-1	5166518	406980
Karangarua-Pit-2	5166429	407250
Karangarua-Pit-3	5166510	407429
Karangarua-Pit-4	5166579	406920
Karangarua-Pit-5	5166581	406921
Karangarua-bedrock	5166440	407258
Karangarua-sed	5174514	403756
Fox-Pit-1	5183804	419019
Fox-Pit-2	5183797	419036
Fox_sed	5185321	418733
Alex-Knob-Pit-2	5192552	431785
Alex-Knob-Pit-3	5192209	431464
Alex_Knob_Pit_4	5192543	431814
Docherty_Creek_sed	5196260	429580
Gunn-Pit-1	5194145	451786
Gunn_Pit_2	5194074	451823
Gunn-Pit-3	5194102	451809
Gunn_Pit_4	5194294	451636
Gunn-Pit-5	5194214	451719
Gunn-Pit-6	5194079	451809
Gunn-Pit-7	5194043	452241
Gunn-Ridge-sed	5194083	452561
Whataroa-sed	5206455	452430
Rapid-Creek-Pit-1	5235916	501425
Rapid-Creek-Pit-2	5236056	501407
Rapid-Creek-Pit-3	5236216	501384
Rapid-Creek-Pit-4	5235974	501423
Rapid-Creek-Pit-5	5236151	501407
Rapid-Creek-sed	5237500	500974
Hokitika_sed	5240528	499687

References

1. T. C. Chamberlin, An attempt to frame a working hypothesis of the cause of glacial periods on an atmospheric basis. *J. Geol.* **7**, 545–584 (1899). [doi:10.1086/608449](https://doi.org/10.1086/608449)
2. M. E. Raymo, W. F. Ruddiman, Tectonic forcing of late Cenozoic climate. *Nature* **359**, 117–122 (1992). [doi:10.1038/359117a0](https://doi.org/10.1038/359117a0)
3. K. L. Ferrier, J. W. Kirchner, Effects of physical erosion on chemical denudation rates: A numerical modeling study of soil mantled hillslopes. *Earth Planet. Sci. Lett.* **272**, 591–599 (2008). [doi:10.1016/j.epsl.2008.05.024](https://doi.org/10.1016/j.epsl.2008.05.024)
4. E. J. Gabet, S. M. Mudd, A theoretical model coupling chemical weathering rates with denudation rates. *Geology* **37**, 151–154 (2009). [doi:10.1130/G25270A.1](https://doi.org/10.1130/G25270A.1)
5. G. E. Hilley, C. P. Chamberlain, S. Moon, S. Porder, S. D. Willett, Competition between erosion and reaction kinetics in controlling silicate-weathering rates. *Earth Planet. Sci. Lett.* **293**, 191–199 (2010). [doi:10.1016/j.epsl.2010.01.008](https://doi.org/10.1016/j.epsl.2010.01.008)
6. A. J. West, Thickness of the chemical weathering zone and implications for erosional and climatic drivers of weathering and for carbon cycle feedbacks. *Geology* **40**, 811–814 (2012). [doi:10.1130/G33041.1](https://doi.org/10.1130/G33041.1)
7. Materials and methods are available as supplementary materials on *Science Online*.
8. R. J. Norris, A. F. Cooper, Late Quaternary slip rates and slip partitioning on the Alpine Fault, New Zealand. *J. Struct. Geol.* **23**, 507–520 (2001). [doi:10.1016/S0191-8141\(00\)00122-X](https://doi.org/10.1016/S0191-8141(00)00122-X)
9. J. M. Tippet, P. J. J. Kamp, Fission track analysis of the Late Cenozoic vertical kinematics of continental Pacific crust, South Island, New Zealand. *J. Geophys. Res.* **98**, (B9), 16119–16148 (1993). [doi:10.1029/92JB02115](https://doi.org/10.1029/92JB02115)
10. N. Hovius, C. P. Stark, P. A. Allen, Sediment flux from a mountain belt derived by landslide mapping. *Geology* **25**, 231–234 (1997). [doi:10.1130/0091-7613\(1997\)025<0231:SFFAMB>2.3.CO;2](https://doi.org/10.1130/0091-7613(1997)025<0231:SFFAMB>2.3.CO;2)
11. D. M. Hicks, U. Shankar, A. I. McKerchar, L. Basher, M. Jessen, I. Lynn, M. Page, Suspended sediment yields from New Zealand rivers. *J. Hydrol. N.Z.* **50**, 81–142 (2011).
12. A. D. Jacobson, J. D. Blum, Relationship between mechanical erosion and atmospheric CO₂ consumption in the New Zealand Southern Alps. *Geology* **31**, 865–868 (2003). [doi:10.1130/G19662.1](https://doi.org/10.1130/G19662.1)
13. G. A. Griffiths, M. J. McSaveney, Distribution of mean annual precipitation across some steep land regions of New Zealand. *N. Z. J. Sci.* **26**, 197–209 (1983).
14. L. R. Basher, P. J. Tonkin, M. J. McSaveney, Geomorphic history of a rapidly uplifting area in a compressional plate boundary: Cropp River, New Zealand. *Z. Geomorphol.* **69**, 117–131 (1988).
15. B. A. Clarke, D. W. Burbank, Quantifying bedrock-fracture patterns within the shallow subsurface: Implications for rock mass strength, bedrock landslides, and erodibility. *J. Geophys. Res.* **116**, (F4), F04009 (2011). [doi:10.1029/2011JF001987](https://doi.org/10.1029/2011JF001987)

16. A. M. Heimsath, W. E. Dietrich, K. Nishiizumi, R. C. Finkel, The soil production function and landscape equilibrium. *Nature* **388**, 358–361 (1997). [doi:10.1038/41056](https://doi.org/10.1038/41056)
17. J. L. Dixon, A. S. Hartshorn, A. M. Heimsath, R. A. DiBiase, K. X. Whipple, Chemical weathering response to tectonic forcing: A soils perspective from the San Gabriel Mountains, California. *Earth Planet. Sci. Lett.* **323-324**, 40–49 (2012). [doi:10.1016/j.epsl.2012.01.010](https://doi.org/10.1016/j.epsl.2012.01.010)
18. C. S. Riebe, J. W. Kirchner, R. C. Finkel, Erosional and climatic effects on long-term chemical weathering rates in granitic landscapes spanning diverse climate regimes. *Earth Planet. Sci. Lett.* **224**, 547–562 (2004). [doi:10.1016/j.epsl.2004.05.019](https://doi.org/10.1016/j.epsl.2004.05.019)
19. J. L. Dixon, F. von Blanckenburg, Soils as pacemakers and limiters of global silicate weathering. *C. R. Geosci.* **344**, 597–609 (2012). [doi:10.1016/j.crte.2012.10.012](https://doi.org/10.1016/j.crte.2012.10.012)
20. J. Braun, F. Herman, G. Batt, Kinematic strain localization. *Earth Planet. Sci. Lett.* **300**, 197–204 (2010). [doi:10.1016/j.epsl.2010.08.018](https://doi.org/10.1016/j.epsl.2010.08.018)
21. J. Beavan, P. Denys, M. Denham, B. Hager, T. Herring, P. Molnar, Distribution of present-day vertical deformation across the Southern Alps, New Zealand, from 10 years of GPS data. *Geophys. Res. Lett.* **37**, L16305 (2010). [doi:10.1029/2010GL044165](https://doi.org/10.1029/2010GL044165)
22. A. M. Heimsath, R. A. DiBiase, K. X. Whipple, Soil production limits and the transition to bedrock-dominated landscapes. *Nat. Geosci.* **5**, 210–214 (2012). [doi:10.1038/ngeo1380](https://doi.org/10.1038/ngeo1380)
23. K. X. Whipple, E. Kirby, S. H. Brocklehurst, Geomorphic limits to climate-induced increases in topographic relief. *Nature* **401**, 39–43 (1999). [doi:10.1038/43375](https://doi.org/10.1038/43375)
24. R. A. DiBiase, A. M. Heimsath, K. X. Whipple, Hillslope response to tectonic forcing in threshold landscapes. *Earth Surf. Process. Landf.* **37**, 855–865 (2012). [doi:10.1002/esp.3205](https://doi.org/10.1002/esp.3205)
25. R. G. Hilton, P. Meunier, N. Hovius, P. J. Bellingham, A. Galy, Landslide impact on organic carbon cycling in a temperate montane forest. *Earth Surf. Process. Landf.* **36**, 1670–1679 (2011). [doi:10.1002/esp.2191](https://doi.org/10.1002/esp.2191)
26. A. Eger, P. C. Almond, L. M. Condrón, Pedogenesis, soil mass balance, phosphorus dynamics and vegetation communities across a Holocene soil chronosequence in a super-humid climate, South Westland, New Zealand. *Geoderma* **163**, 185–196 (2011). [doi:10.1016/j.geoderma.2011.04.007](https://doi.org/10.1016/j.geoderma.2011.04.007)
27. Z.-X. Tsai, G. J.-Y. You, H.-Y. Lee, Y.-J. Chiu, Modeling the sediment yield from landslides in the Shihmen Reservoir watershed, Taiwan. *Earth Surf. Process. Landf.* **38**, 661–674 (2013). [doi:10.1002/esp.3309](https://doi.org/10.1002/esp.3309)
28. I. J. Larsen, D. R. Montgomery, Landslide erosion coupled to tectonics and river incision. *Nat. Geosci.* **5**, 468–473 (2012). [doi:10.1038/ngeo1479](https://doi.org/10.1038/ngeo1479)
29. J. D. Milliman, K. L. Farnsworth, *River Discharge to the Coastal Ocean: A Global Synthesis* (Cambridge Univ. Press, New York, 2011).
30. W. B. Lyons, A. E. Carey, D. M. Hicks, C. A. Nezat, Chemical weathering in high-sediment-yielding watersheds, New Zealand. *J. Geophys. Res.* **110**, (F1), F01008 (2005). [doi:10.1029/2003JF000088](https://doi.org/10.1029/2003JF000088)

31. E. Gabet, A theoretical model coupling chemical weathering and physical erosion in landslide-dominated landscapes. *Earth Planet. Sci. Lett.* **264**, 259–265 (2007). [doi:10.1016/j.epsl.2007.09.028](https://doi.org/10.1016/j.epsl.2007.09.028)
32. J. Moore, A. D. Jacobson, C. Holmden, D. Craw, Tracking the relationship between mountain uplift, silicate weathering, and long-term CO₂ consumption with Ca isotopes: Southern Alps, New Zealand. *Chem. Geol.* **341**, 110–127 (2013). [doi:10.1016/j.chemgeo.2013.01.005](https://doi.org/10.1016/j.chemgeo.2013.01.005)
33. E. G. Green, W. E. Dietrich, J. F. Banfield, Quantification of chemical weathering rates across an actively eroding hillslope. *Earth Planet. Sci. Lett.* **242**, 155–169 (2006). [doi:10.1016/j.epsl.2005.11.039](https://doi.org/10.1016/j.epsl.2005.11.039)
34. K. Yoo, R. Amundson, A. M. Heimsath, W. E. Dietrich, G. H. Brimhall, Integration of geochemical mass balance with sediment transport to calculate rates of soil chemical weathering and transport on hillslopes. *J. Geophys. Res.* **112**, (F2), F02013 (2007). [doi:10.1029/2005JF000402](https://doi.org/10.1029/2005JF000402)
35. R. Burt, Ed., Soil Survey Investigations Report No. 51, Version 1.0, Natural Resources Conservation Service, U.S. Department of Agriculture, 407 pp. (2009).
36. J. O. Stone, *Extraction of Al and Be from quartz for isotopic analysis*, <http://depts.washington.edu/cosmolab/chem/Al-26_Be-10.pdf> (2001).
37. R. Ditchburn, N. Whitehead, The separation of ¹⁰Be from silicates, in *3rd workshop of the South Pacific Environmental Radioactivity Association*, pp. 4–7 (1994).
38. C. S. Riebe, J. W. Kirchner, D. E. Granger, R. C. Finkel, Strong tectonic and weak climatic control of long-term chemical weathering rates. *Geology* **29**, 511–514 (2001). [doi:10.1130/0091-7613\(2001\)029<0511:STAWCC>2.0.CO;2](https://doi.org/10.1130/0091-7613(2001)029<0511:STAWCC>2.0.CO;2)
39. K. L. Ferrier, J. W. Kirchner, R. C. Finkel, Weak influences of climate and mineral supply rates on chemical erosion rates: Measurements along two altitudinal transects in the Idaho Batholith. *J. Geophys. Res.* **117**, (F2), F02026 (2012). [doi:10.1029/2011JF002231](https://doi.org/10.1029/2011JF002231)
40. H. W. Nesbitt, G. M. Young, Early Proterozoic climates and plate motions inferred from major element chemistry of lutites. *Nature* **299**, 715–717 (1982). [doi:10.1038/299715a0](https://doi.org/10.1038/299715a0)
41. G. H. Brimhall, C. J. Lewis, J. J. Ague, W. E. Dietrich, J. Hampel, T. Teague, P. Rix, Metal enrichment in bauxites by deposition of chemically mature eolian dust. *Nature* **333**, 819–824 (1988). [doi:10.1038/333819a0](https://doi.org/10.1038/333819a0)
42. K. L. Ferrier, J. W. Kirchner, R. C. Finkel, Estimating millennial-scale rates of dust incorporation into eroding hillslope regolith using cosmogenic nuclides and immobile weathering tracers. *J. Geophys. Res.* **116**, (F3), F03022 (2011). [doi:10.1029/2011JF001991](https://doi.org/10.1029/2011JF001991)
43. A. C. Kurtz, L. A. Derry, O. A. Chadwick, M. J. Alfano, Refractory element mobility in volcanic soils. *Geology* **28**, 683–686 (2000). [doi:10.1130/0091-7613\(2000\)28<683:REMIVS>2.0.CO;2](https://doi.org/10.1130/0091-7613(2000)28<683:REMIVS>2.0.CO;2)
44. M. E. Hodson, Experimental evidence for mobility of Zr and other trace elements in soils. *Geochim. Cosmochim. Acta* **66**, 819–828 (2002). [doi:10.1016/S0016-7037\(01\)00803-1](https://doi.org/10.1016/S0016-7037(01)00803-1)

45. D. E. Granger, J. W. Kirchner, R. Finkel, Spatially averaged long-term erosion rates measured from in situ-produced cosmogenic nuclides in alluvial sediment. *J. Geol.* **104**, 249–257 (1996). [doi:10.1086/629823](https://doi.org/10.1086/629823)
46. D. E. Granger, C. S. Riebe, Cosmogenic nuclides in weathering and erosion, in *Treatise on Geochemistry*, vol. 5, J. Drever, Ed. (Elsevier, London, 2007).
47. M. C. Jungers, P. R. Bierman, A. Matmon, K. Nichols, J. Larsen, R. Finkel, Tracing hillslope sediment production and transport with in situ and meteoric ^{10}Be . *J. Geophys. Res.* **114**, (F4), F04020 (2009). [doi:10.1029/2008JF001086](https://doi.org/10.1029/2008JF001086)
48. E. T. Brown, F. Colin, D. L. Bourlès, Quantitative evaluation of soil processes using in situ-produced cosmogenic nuclides. *C. R. Geosci.* **335**, 1161–1171 (2003). [doi:10.1016/j.crte.2003.10.004](https://doi.org/10.1016/j.crte.2003.10.004)
49. E. T. Brown, R. F. Stallard, M. C. Larsen, G. M. Raisbeck, F. Yiou, Denudation rates determined from the accumulation of in situ-produced ^{10}Be in the Luquillo Experimental Forest, Puerto Rico. *Earth Planet. Sci. Lett.* **129**, 193–202 (1995). [doi:10.1016/0012-821X\(94\)00249-X](https://doi.org/10.1016/0012-821X(94)00249-X)
50. P. Bierman, E. J. Steig, Estimating rates of denudation using cosmogenic isotope abundances in sediment. *Earth Surf. Process. Landf.* **21**, 125–139 (1996). [doi:10.1002/\(SICI\)1096-9837\(199602\)21:2<125::AID-ESP511>3.0.CO;2-8](https://doi.org/10.1002/(SICI)1096-9837(199602)21:2<125::AID-ESP511>3.0.CO;2-8)
51. D. Lal, Cosmic ray labeling of erosion surfaces: In situ nuclide production rates and erosion models. *Earth Planet. Sci. Lett.* **104**, 424–439 (1991). [doi:10.1016/0012-821X\(91\)90220-C](https://doi.org/10.1016/0012-821X(91)90220-C)
52. E. E. Small, R. S. Anderson, J. L. Repka, R. Finkel, Erosion rates of alpine bedrock summit surfaces deduced from in situ ^{10}Be and ^{26}Al . *Earth Planet. Sci. Lett.* **150**, 413–425 (1997). [doi:10.1016/S0012-821X\(97\)00092-7](https://doi.org/10.1016/S0012-821X(97)00092-7)
53. J. J. Roering, J. W. Kirchner, W. E. Dietrich, Hillslope evolution by nonlinear, slope-dependent transport: Steady state morphology and equilibrium adjustment timescales. *J. Geophys. Res. Solid Earth* **106**, (B8), 16499–16513 (2001). [doi:10.1029/2001JB000323](https://doi.org/10.1029/2001JB000323)
54. D. W. Burbank, J. Leland, E. Fielding, R. S. Anderson, N. Brozovic, M. R. Reid, C. Duncan, Bedrock incision, rock uplift and threshold hillslopes in the northwestern Himalayas. *Nature* **379**, 505–510 (1996). [doi:10.1038/379505a0](https://doi.org/10.1038/379505a0)
55. A. Reif, R. B. Allen, Plant communities of the steepland conifer-broadleaved hardwood forests of central Westland, South Island, New Zealand. *Phytocoenologia* **16**, 145–224 (1988).
56. J. Harrison, Soil distribution and landscape dynamics, Camp Creek, Westland, in *Proceedings of the soil dynamics and land use seminar*. I. B. Campbell, Ed. New Zealand Society of Soil Science, Lower Hutt, and New Zealand Soil Conservators Association, 65–77 (1985).
57. I. J. Larsen, D. R. Montgomery, O. Korup, Landslide erosion controlled by hillslope material. *Nat. Geosci.* **3**, 247–251 (2010). [doi:10.1038/ngeo776](https://doi.org/10.1038/ngeo776)

58. P. Meunier, N. Hovius, J. A. Haines, Topographic site effects and the location of earthquake induced landslides. *Earth Planet. Sci. Lett.* **275**, 221–232 (2008). [doi:10.1016/j.epsl.2008.07.020](https://doi.org/10.1016/j.epsl.2008.07.020)
59. R. Sutherland, D. Eberhart-Phillips, R. A. Harris, T. Stern, J. Beavan, S. Ellis, S. Henrys, S. Cox, R. J. Norris, K. R. Berryman, J. Townend, S. Bannister, J. Pettinga, B. Leitner, L. Wallace, T. A. Little, A. F. Cooper, M. Yetton, M. Stirling, Do great earthquakes occur on the Alpine Fault in central South Island, New Zealand? *Geophysical Monograph Series* **175**, 235–251 (2007). [doi:10.1029/175GM12](https://doi.org/10.1029/175GM12)
60. A. M. Heimsath, W. E. Dietrich, K. Nishiizumi, R. Finkel, Stochastic processes of soil production and transport: Erosion rates, topographic variation and cosmogenic nuclides in the Oregon Coast Range. *Earth Surf. Process. Landf.* **26**, 531–552 (2001). [doi:10.1002/esp.209](https://doi.org/10.1002/esp.209)
61. J. J. Roering, J. Marshall, A. M. Booth, M. Mort, Q. Jin, Evidence for biotic controls on topography and soil production. *Earth Planet. Sci. Lett.* **298**, 183–190 (2010). [doi:10.1016/j.epsl.2010.07.040](https://doi.org/10.1016/j.epsl.2010.07.040)
62. E. J. Gabet, S. M. Mudd, Bedrock erosion by root fracture and tree throw: A coupled biogeomorphic model to explore the humped soil production function and the persistence of hillslope soils. *J. Geophys. Res.* **115**, (F4), F04005 (2010). [doi:10.1029/2009JF001526](https://doi.org/10.1029/2009JF001526)
63. L. J. Reinhardt, T. B. Hoey, T. T. Barrows, T. J. Dempster, P. Bishop, L. K. Fifield, Interpreting erosion rates from cosmogenic radionuclide concentrations measured in rapidly eroding terrain. *Earth Surf. Process. Landf.* **32**, 390–406 (2007). [doi:10.1002/esp.1415](https://doi.org/10.1002/esp.1415)
64. G. Balco, J. Briner, R. C. Finkel, J. A. Rayburn, J. C. Ridge, J. M. Schaefer, Regional beryllium-10 production rate calibration for late-glacial northeastern North America. *Quat. Geochronol.* **4**, 93–107 (2009). [doi:10.1016/j.quageo.2008.09.001](https://doi.org/10.1016/j.quageo.2008.09.001)
65. A. E. Putnam, J. M. Schaefer, D. J. A. Barrell, M. Vandergoes, G. H. Denton, M. R. Kaplan, R. C. Finkel, R. Schwartz, B. M. Goehring, S. E. Kelley, In situ cosmogenic ^{10}Be production-rate calibration from the Southern Alps, New Zealand. *Quat. Geochronol.* **5**, 392–409 (2010). [doi:10.1016/j.quageo.2009.12.001](https://doi.org/10.1016/j.quageo.2009.12.001)
66. J. A. McKean, W. E. Dietrich, R. C. Finkel, J. R. Southon, M. W. Caffee, Quantification of soil production and downslope creep rates from cosmogenic ^{10}Be accumulations on a hillslope profile. *Geology* **21**, 343–346 (1993). [doi:10.1130/0091-7613\(1993\)021<0343:QOSPAD>2.3.CO;2](https://doi.org/10.1130/0091-7613(1993)021<0343:QOSPAD>2.3.CO;2)
67. J. D. Phillips, A. V. Turkington, D. A. Marion, Weathering and vegetation effects in early stages of soil formation. *Catena* **72**, 21–28 (2008). [doi:10.1016/j.catena.2007.03.020](https://doi.org/10.1016/j.catena.2007.03.020)
68. N. A. Niemi, M. Oskin, D. W. Burbank, A. M. Heimsath, E. J. Gabet, Effects of bedrock landslides on cosmogenically determined erosion rates. *Earth Planet. Sci. Lett.* **237**, 480–498 (2005). [doi:10.1016/j.epsl.2005.07.009](https://doi.org/10.1016/j.epsl.2005.07.009)
69. B. J. Yanites, G. E. Tucker, R. S. Anderson, Numerical and analytical models of cosmogenic radionuclide dynamics in landslide-dominated drainage basins. *J. Geophys. Res.* **114**, (F1), F01007 (2009). [doi:10.1029/2008JF001088](https://doi.org/10.1029/2008JF001088)

70. F. Herman, E. J. Rhodes, J. Braun, L. Heiniger, Uniform erosion rates and relief amplitude during glacial cycles in the Southern Alps of New Zealand, as revealed from OSL-thermochronology. *Earth Planet. Sci. Lett.* **297**, 183–189 (2010). [doi:10.1016/j.epsl.2010.06.019](https://doi.org/10.1016/j.epsl.2010.06.019)
71. G. Balco, J. O. Stone, N. A. Lifton, T. J. Dunai, A complete and easily accessible means of calculating surface exposure ages or erosion rates from ^{10}Be and ^{26}Al measurements. *Quat. Geochronol.* **3**, 174–195 (2008). [doi:10.1016/j.quageo.2007.12.001](https://doi.org/10.1016/j.quageo.2007.12.001)
72. S. A. Binnie, W. M. Phillips, M. A. Summerfield, L. K. Fifield, Sediment mixing and basin-wide cosmogenic nuclide analysis in rapidly eroding mountainous environments. *Quat. Geochronol.* **1**, 4–14 (2006). [doi:10.1016/j.quageo.2006.06.013](https://doi.org/10.1016/j.quageo.2006.06.013)
73. J. O. Stone, Air pressure and cosmogenic isotope production. *J. Geophys. Res. Solid Earth* **105**, (B10), 23753–23759 (2000). [doi:10.1029/2000JB900181](https://doi.org/10.1029/2000JB900181)
74. E. E. Small, R. S. Anderson, G. S. Hancock, Estimates of the rate of regolith production using ^{10}Be and ^{26}Al from an alpine hillslope. *Geomorphology* **27**, 131–150 (1999). [doi:10.1016/S0169-555X\(98\)00094-4](https://doi.org/10.1016/S0169-555X(98)00094-4)
75. C. S. Riebe, J. W. Kirchner, D. E. Granger, Quantifying quartz enrichment and its consequences for cosmogenic measurements of erosion rates from alluvial sediment and regolith. *Geomorphology* **40**, 15–19 (2001). [doi:10.1016/S0169-555X\(01\)00031-9](https://doi.org/10.1016/S0169-555X(01)00031-9)
76. I. J. Larsen, Hillslope erosion and weathering rates in Earth's most rapidly uplifting mountains. Ph.D. dissertation, University of Washington, 128 p. (2013).
77. J. J. Owen, R. Amundson, W. E. Dietrich, K. Nishiizumi, B. Sutter, G. Chong, The sensitivity of hillslope bedrock erosion to precipitation. *Earth Surf. Process. Landf.* **36**, 117–135 (2011). [doi:10.1002/esp.2083](https://doi.org/10.1002/esp.2083)
78. J. L. Dixon, A. M. Heimsath, J. Kaste, R. Amundson, Climate-driven processes of hillslope weathering. *Geology* **37**, 975–978 (2009). [doi:10.1130/G30045A.1](https://doi.org/10.1130/G30045A.1)
79. A. M. Heimsath, J. Chappell, W. E. Dietrich, K. Nishiizumi, R. C. Finkel, Late Quaternary erosion in southeastern Australia: A field example using cosmogenic nuclides. *Quat. Int.* **83**, 169–185 (2001). [doi:10.1016/S1040-6182\(01\)00038-6](https://doi.org/10.1016/S1040-6182(01)00038-6)
80. A. M. Heimsath, J. Chappell, W. E. Dietrich, K. Nishiizumi, R. C. Finkel, Soil production on a retreating escarpment in southeastern Australia. *Geology* **28**, 787–790 (2000). [doi:10.1130/0091-7613\(2000\)28<787:SPOARE>2.0.CO;2](https://doi.org/10.1130/0091-7613(2000)28<787:SPOARE>2.0.CO;2)
81. A. M. Heimsath, D. J. Furbish, W. E. Dietrich, The illusion of diffusion: Field evidence for depth-dependent sediment transport. *Geology* **33**, 949–952 (2005). [doi:10.1130/G21868.1](https://doi.org/10.1130/G21868.1)
82. A. Heimsath, D. Fink, G. R. Hancock, The 'humped' soil production function: Eroding Arnhem Land, Australia. *Earth Surf. Process. Landf.* **34**, 1674–1684 (2009). [doi:10.1002/esp.1859](https://doi.org/10.1002/esp.1859)
83. B. C. Burke, A. M. Heimsath, A. F. White, Coupling chemical weathering with soil production across soil-mantled landscapes. *Earth Surf. Process. Landf.* **32**, 853–873 (2007). [doi:10.1002/esp.1443](https://doi.org/10.1002/esp.1443)

84. B. C. Burke, A. M. Heimsath, J. L. Dixon, J. Chappell, K. Yoo, Weathering the escarpment: Chemical and physical rates and processes, south-eastern Australia. *Earth Surf. Process. Landf.* **34**, 768–785 (2009). [doi:10.1002/esp.1764](https://doi.org/10.1002/esp.1764)
85. K. P. Norton, F. von Blanckenburg, Silicate weathering of soil-mantled slopes in an active Alpine landscape. *Geochim. Cosmochim. Acta* **74**, 5243–5258 (2010). [doi:10.1016/j.gca.2010.06.019](https://doi.org/10.1016/j.gca.2010.06.019)
86. J. L. Dixon, A. M. Heimsath, R. Amundson, The critical role of climate and saprolite weathering in landscape evolution. *Earth Surf. Process. Landf.* **34**, 1507–1521 (2009). [doi:10.1002/esp.1836](https://doi.org/10.1002/esp.1836)
87. C. S. Riebe, D. E. Granger, Quantifying effects of deep and near-surface chemical erosion on cosmogenic nuclides in soils, saprolite, and sediment. *Earth Surf. Process. Landf.* **38**, 523–533 (2013). [doi:10.1002/esp.3339](https://doi.org/10.1002/esp.3339)
88. J. J. Roering, How well can hillslope evolution models ‘explain’ topography? Simulating soil transport and production with high-resolution topographic data. *Geol. Soc. Am. Bull.* **120**, 1248–1262 (2008). [doi:10.1130/B26283.1](https://doi.org/10.1130/B26283.1)
89. M. D. Hurst, S. M. Mudd, R. C. Walcott, M. Attal, K. Yoo, Using hilltop curvature to derive the spatial distribution of erosion rates. *J. Geophys. Res.* **117**, (F2), F02017 (2012). [doi:10.1029/2011JF002057](https://doi.org/10.1029/2011JF002057)
90. A. C. Beck, Gravity faulting as a mechanism of topographic adjustment. *N.Z. J. Geol. Geophys.* **11**, 191–199 (1968). [doi:10.1080/00288306.1968.10423684](https://doi.org/10.1080/00288306.1968.10423684)
91. O. Korup, Large landslides and their effect on sediment flux in South Westland, New Zealand. *Earth Surf. Process. Landf.* **30**, 305–323 (2005). [doi:10.1002/esp.1143](https://doi.org/10.1002/esp.1143)
92. M. W. Hughes, P. C. Almond, J. J. Roering, Increased sediment transport via bioturbation at the last glacial-interglacial transition. *Geology* **37**, 919–922 (2009). [doi:10.1130/G30159A.1](https://doi.org/10.1130/G30159A.1)